

## Fickian yet non-Gaussian diffusion in two-dimensional Yukawa liquids

Zahra Ghannad<sup>1</sup>\*

*Department of Physics, Alzahra University, P.O. Box 19938-93973, Tehran, Iran*

 (Received 5 August 2019; published 25 September 2019)

We investigate Fickian diffusion in two-dimensional (2D) Yukawa liquids using molecular dynamics simulations. We compute the self-van Hove correlation function  $G_s(r, t)$  and the self-intermediate scattering function  $F_s(k, t)$ , and we compare these functions with those obtained from mean-squared displacement (MSD) using the Gaussian approximation. According to this approximation, a linear MSD with time implies a Gaussian behavior for  $G_s(r, t)$  and  $F_s(k, t)$  at all times. Surprisingly, we find that these functions deviate from Gaussian at intermediate timescales, indicating the failure of the Gaussian approximation. Furthermore, we quantify these deviations by the non-Gaussian parameter, and we find that the deviations increase when the temperature of the liquid decreases. The origin of the non-Gaussian behavior may be the heterogeneous dynamics of dust particles observed in 2D Yukawa liquids.

DOI: [10.1103/PhysRevE.100.033211](https://doi.org/10.1103/PhysRevE.100.033211)

### I. INTRODUCTION

Dusty plasma is a weakly ionized gas containing ions, electrons, neutrals, and highly charged dust particles [1–5]. In the laboratory, due to the electric field in the plasma sheath, dust particles can be levitated and confined. Therefore, they can be floated in a monolayer, with an ignorable out-of-plane motion to form a two-dimensional (2D) dusty plasma [6–8]. Because of shielding by electrons and ions of the background plasma, the interaction potential between dust particles is accurately described by the Yukawa potential, i.e.,  $\phi(r) = Q^2 \exp(-r/\lambda_D)/4\pi\epsilon_0 r$ , where  $\lambda_D$  is the Debye shielding length and  $Q$  is the dust charge [9,10]. The high charges of dust particles cause their electrostatic potential energy to exceed the kinetic energy. Hence, dust particles are strongly coupled so that the collection of particles exhibits behaviors of liquids [6–8] and solids [11,12]. Here, we focus on the Brownian diffusion of dust particles in 2D equilibrium Yukawa liquids.

The random motion of dust particles in 2D Yukawa liquids can be described by Brownian diffusion [13]. It was observed by Brown [14], and its theoretical description was derived by Einstein [15]. There are two fundamental features with Brownian diffusion [16]:

(i) The mean-squared displacement  $\langle \Delta r^2(t) \rangle$  is linear with time,

$$\langle [\Delta r(t)]^2 \rangle = \langle |\mathbf{r}(t) - \mathbf{r}(0)|^2 \rangle = \int r^2 G_s(\mathbf{r}, t) d\mathbf{r} = 2dDt, \quad (1)$$

which is called Fickian (normal) diffusion. Here,  $D$  is the diffusion coefficient and  $d$  denotes the dimension.

(ii) The self-part of the van Hove correlation function, i.e., the distribution of the particle displacement, is Gaussian:

$$G_s(\mathbf{r}, t) = \frac{1}{(4\pi Dt)^{d/2}} \exp\left(-\frac{\mathbf{r}^2}{4Dt}\right). \quad (2)$$

$G_s(\mathbf{r}, t) d\mathbf{r}$  gives the probability of finding a particle at position  $\mathbf{r}$  at time  $t$  given that the same particle was at the origin at the initial time  $t = 0$  [17–19].

In this work, by molecular dynamics (MD) simulation, we investigate the diffusion process in 2D equilibrium Yukawa liquids. Investigating the diffusion in 2D Yukawa liquids has attracted a great deal of interest over the past decade [20–31]. We find that the distribution function of dust particle displacement  $G_s(r, t)$  is not Gaussian as we expected for a Fickian diffusion, while the mean-squared displacement appears Fickian (linear with time). Fickian yet non-Gaussian diffusions have also been observed in various systems, such as colloids [32–35] and porous media [36,37].

The paper is organized as follows. In Sec. II, we describe the fundamental features of the simulation technique to mimic 2D Yukawa liquids. In Sec. III, we compute four diagnostics including the mean-squared displacement, the self-part of the van Hove correlation function, the non-Gaussian parameter, and the self-part of the intermediate scattering function to interpret the underlying physics. In Sec. IV, we present the conclusions.

### II. MODEL AND SIMULATION TECHNIQUE

To study 2D equilibrium Yukawa liquids, we performed equilibrium MD simulations [38]. We integrated the equation of motion  $m\ddot{\mathbf{r}}_i = -\nabla \sum_j \phi_{ij}$  for  $N = 1024$  particles, where  $\phi_{ij}$  is the Yukawa pair interaction potential [9,10]. An equilibrium Yukawa system can be characterized by two dimensionless parameters [22,39]:

(i) The Coulomb coupling parameter  $\Gamma = Q^2/4\pi\epsilon_0 a k_B T$ , where  $\epsilon_0$  is the dielectric constant,  $k_B$  is the Boltzmann constant,  $Q$  is the charge of a dust particle,  $T$  is the kinetic temperature of dust particles,  $a = (n\pi)^{-1/2}$  is the Wigner-Seitz radius for 2D systems, and  $n$  is the surface number density of dust particles.

(ii) The screening parameter  $\kappa = a/\lambda_D$ .

\*z.ghannad@alzahra.ac.ir

TABLE I. Dimensionless units for 2D Yukawa liquids.

Quantity	Symbol		Dimensionless unit
Length	$r$	$\rightarrow$	$r/a$
Time	$t$	$\rightarrow$	$\omega_{pd}t$
Temperature	$T$	$\rightarrow$	$\Gamma^{-1}$
Surface number density	$n$	$\rightarrow$	$na^2$
Potential energy	$\phi$	$\rightarrow$	$\phi/a^2\omega_{pd}^2$
Wave number	$k$	$\rightarrow$	$ka$

The dimensionless units in this work are listed in Table I, where  $\omega_{pd} = (Q^2/2\pi\epsilon_0ma^3)^{1/2}$  is the nominal 2D dusty plasma frequency [40].

The values of  $\Gamma$  and  $\kappa$  are entered as input parameters in simulations. We chose three values of  $\kappa = 0.5, 1.2,$  and  $2.0$  as the beginning, the middle, and the end of the allowed interval from an experimentally relevant range of  $0.5 \leq \kappa \leq 2.0$  [41]. For each  $\kappa$  value, there is one specific melting point  $\Gamma_m$ , so that for  $\Gamma < \Gamma_m$ , the 2D Yukawa system is in the liquid phase as reported by Hartmann *et al.* [42]. These values are  $\Gamma_m = 142$  for  $\kappa = 0.5$  [5,42],  $\Gamma_m = 200$  for  $\kappa = 1.2$  [42], and  $\Gamma_m = 415$  for  $\kappa = 2.0$  [21,42]. In simulations, we chose the values of  $\Gamma$  over a range that allows simulations of liquids.

The simulation box is a rectangular box with a size of  $61.1a \times 52.9a$ , so that the surface number density is consistent with the definition of the Wigner-Seitz radius, i.e.,  $n = 1024/(61.1a \times 52.9a) \approx 1/(\pi a^2)$  [43]. To eliminate boundary effects caused by the finite size of the simulation box, and to model the system as an infinite one, we applied the periodic boundary conditions.

We began from an initial random configuration of dust particles and used a Nosé-Hoover thermostat [44,45] to reach the system at the desired temperature. Then, we turned off the thermostat to sample the dynamical properties.

We used the velocity Verlet algorithm [46] to integrate the equations of motion with the integration time step of  $0.037\omega_{pd}^{-1}$ , and we verified that this time step is adequately small to conserve energy. Generally, the time step is chosen from the range between  $[0.0037$  and  $0.037] \omega_{pd}^{-1}$  depending on the  $\Gamma$  values; i.e.,  $0.0037\omega_{pd}^{-1}$  for  $1.0 \leq \Gamma < 4.0$ ,  $0.0093\omega_{pd}^{-1}$  for  $4.0 \leq \Gamma < 10.0$ ,  $0.0185\omega_{pd}^{-1}$  for  $10.0 \leq \Gamma < 40.0$ , and  $0.037\omega_{pd}^{-1}$  for  $\Gamma \geq 40.0$  [6]. The last one is chosen in our simulations because we studied  $\Gamma > 100$ .

Since the Yukawa potential decays as  $\exp(-r)/r$ , the cut-off radius for this potential in MD simulations should be sufficiently large to ensure that the perturbation introduced into the simulations due to the potential truncation is negligible [1]. We truncated the Yukawa potential at  $r_{cut} = 24.8a$ , as in [6–8].

To verify that our MD simulations reasonably modeled a canonical ensemble in thermal equilibrium, we applied a standard test as follows:

In a finite system in equilibrium, the temperature fluctuates about the mean value, i.e.,  $\delta T = T - \langle T \rangle$ . If the system exhibits canonical fluctuations (within a computationally reasonable time), then the variance of the temperature is [47]

$$\langle (\delta T)^2 \rangle = \frac{2 \langle T \rangle^2}{d N}, \quad (3)$$

where  $\langle T \rangle$  is the mean temperature. We calculated the variance of the temperature in our simulations and compared it to the variance for the canonical ensemble in thermal equilibrium, given in the above equation. According to the standard test, the ratio of these two variances is unity for a canonical system in thermal equilibrium. Although a value of unity is an ideal value, in a simulation due to a limited time range for sampling, a value very close to 1 is considered successful. We found that the ratio was 0.996, which assured us our simulations precisely modeled a canonical system in equilibrium.

### III. RESULTS AND DISCUSSIONS

In this section, we use four diagnostics to characterize the dynamics of dust particles in 2D Yukawa liquids. They are the mean-squared displacement, the self-part of the van Hove correlation function, the non-Gaussian parameter, and the self-intermediate scattering function, as explained below.

#### A. Mean-squared displacement

The first diagnostic, namely mean-squared displacement (MSD),  $\langle [\Delta r(t)]^2 \rangle = \langle |\mathbf{r}_i(t) - \mathbf{r}_i(0)|^2 \rangle$ , is calculated to identify Fickian (normal) diffusion. Here,  $\mathbf{r}_i(t)$  is the position of particle  $i$  at time  $t$ , and  $\langle \dots \rangle$  denotes an ensemble average. For a 2D system, the MSD obeys a power law  $\text{MSD}(t) \propto 4Dt^\alpha$ . When MSD is plotted as a function of time in a log-log plot, the fitted curve with a straight line gives the slope  $\alpha$ . The signatures of normal diffusion and anomalous diffusion are  $\alpha = 1$  and  $\alpha \neq 1$ , respectively. Anomalous diffusion refers to both superdiffusion ( $\alpha > 1$ ) and subdiffusion ( $\alpha < 1$ ). Since data from simulations will never yield a value that is exactly 1, a range of  $0.9 < \alpha < 1.1$  is classified as normal diffusion, and  $\alpha > 1.1$  for superdiffusion [20,29,48].

Results for MSD with selected values of  $\kappa$  and  $\Gamma$  are shown as a function of time in a log-log scale in Figs. 1(a)–1(c). At very short times ( $\omega_{pd}t \lesssim 5$ ) when dust particles move in the cage created by neighboring dust particles, all curves are fitted by a straight line with a slope  $\alpha = 2$ , indicating the ballistic motion. At later times, dust particles escape from the cages and diffuse. Here we are interested in motion at intermediate times (when the Gaussian approximation fails). For a period of  $100 < \omega_{pd}t < 600$ , the fitting results of the exponent  $\alpha$  for  $\kappa = 0.5$  are  $\alpha = 1.15$  for  $\Gamma = 100$ ,  $\alpha = 1.08$  for  $\Gamma = 120$ , and  $\alpha = 1.05$  for  $\Gamma = 130$ . These results for  $\kappa = 1.2$  are  $\alpha = 1.15$  for  $\Gamma = 100$ ,  $\alpha = 1.11$  for  $\Gamma = 140$ , and  $\alpha = 1.05$  for  $\Gamma = 190$ . For  $\kappa = 2.0$ , we obtain  $\alpha = 1.09$  for  $\Gamma = 240$ ,  $\alpha = 1.07$  for  $\Gamma = 320$ , and  $\alpha = 1.04$  for  $\Gamma = 400$ . All these results indicate that with increasing  $\Gamma$  (equivalently decreasing temperature) to near  $\Gamma_m$  ( $T_m$ ), superdiffusion of dust particles tends to normal diffusion. Therefore, for very low temperatures, i.e., supercooled Yukawa liquids ( $\Gamma > 120$  for  $\kappa = 0.5$ ,  $\Gamma > 140$  for  $\kappa = 1.2$ ,  $\Gamma > 320$  for  $\kappa = 2.0$ ), the diffusion of dust particles is normal (Fickian) with good accuracy.

#### B. Self-part of the van Hove correlation function

The self-part of the van Hove correlation function, i.e., the distribution of the particle displacement, is defined as [19]

$$G_s(\mathbf{r}, t) = \frac{1}{N} \left\langle \sum_{i=1}^N \delta(\mathbf{r} - \mathbf{r}_i(t) + \mathbf{r}_i(0)) \right\rangle, \quad (4)$$

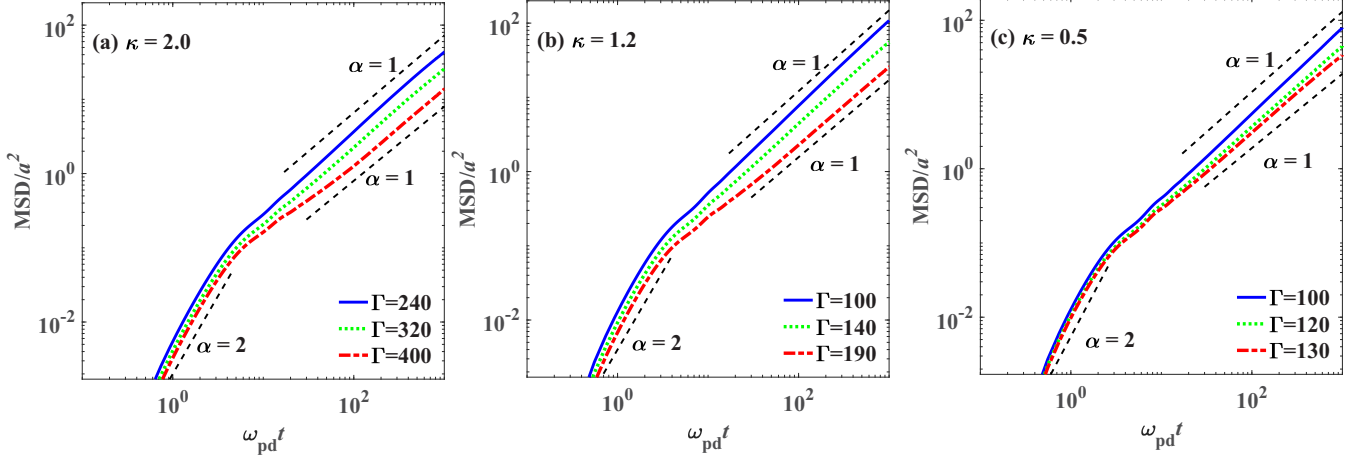


FIG. 1. Mean-squared displacements  $\langle [\Delta r(t)]^2 \rangle$  for different temperatures. (a)  $\kappa = 2.0$ , (b)  $\kappa = 1.2$ , and (c)  $\kappa = 0.5$ . At short times, MSD  $\propto t^2$ . At later times, when  $100 < \omega_{pd} t < 600$ , MSD  $\propto t^\alpha$ , where  $\alpha$  comes very close to 1 with decreasing temperature (increasing  $\Gamma$ ), indicating Fickian diffusion.

where  $\langle \dots \rangle$  represents an ensemble average, and  $\delta$  is the Dirac delta function. For isotropic liquids,  $G_s$  depends only on the scalar distance,  $r = |\mathbf{r}|$ . Thus, Eq. (4) reduces to

$$G_s(r, t) = \frac{1}{N} \left\langle \sum_{i=1}^N \delta(r - |r_i(t) - r_i(0)|) \right\rangle. \quad (5)$$

Physically,  $2\pi r G_s(r, t) dr$  measures the probability of finding a dust particle at distance  $r$  from an origin at time  $t$  given that the same dust particle was at the origin at the initial time  $t = 0$  [19]. Thus,  $G_s(r, t)$  is normalized by

$$\int G_s(r, t) d\mathbf{r} = 1. \quad (6)$$

Figures 2(a)–2(c), 3(a)–3(c), and 4(a)–4(c) show the time evolution of the normalized  $G_s(r, t)$  for the selected  $\kappa$  and  $\Gamma$  values, and compare  $G_s(r, t)$  with Gaussian distribution  $G_s^{\text{Gauss}}(r, t)$  (solid lines) obtained from Eq. (2), i.e.,  $G_s^{\text{Gauss}}(r, t) = \{1/\pi \langle [\Delta r(t)]^2 \rangle\} \exp\{-r^2/\langle [\Delta r(t)]^2 \rangle\}$ , where  $\langle [\Delta r(t)]^2 \rangle$  is obtained from the simulation. At intermediate times, when the MSD is linear with time,  $G_s(r, t)$  functions deviate from the Gaussian.

How much difference is between  $G_s(r, t)$  and the Gaussian distribution? To answer this question, we calculate the relative difference between  $G_s(r, t)$  and  $G_s^{\text{Gauss}}(r, t)$ , i.e.,  $G_s(r, t) - G_s^{\text{Gauss}}(r, t)/G_s^{\text{Gauss}}(r, t)$  as shown in Figs. 5(a)–5(c), 6(a)–6(c), and 7(a)–7(c). Maximum relative differences between  $G_s(r, t)$  and  $G_s^{\text{Gauss}}(r, t)$  become as large as 10,  $10^3$ , and  $10^4$  for  $\kappa = 2$ ,  $\Gamma = 240, 320$ , and 400, respectively; 10,  $10^2$ , and  $10^3$  for  $\kappa = 1.2$ ,  $\Gamma = 100, 140$ , and 190, respectively; and 10,  $10^2$ , and  $10^2$  for  $\kappa = 0.5$ ,  $\Gamma = 100, 120$ , and 130, respectively.

For a fixed value of  $\kappa$ , the maximum relative difference increases with increasing  $\Gamma$ , i.e., with decreasing  $T$ , and it is as large as  $10^4$ , which belongs to the lowest temperature, i.e.,  $T = 0.0025$  or  $\Gamma = 400$  [see Fig. 5(c)]. This means that in the supercooled 2D Yukawa liquids, the distribution function of dust particle displacement has the biggest discrepancy from the Gaussian distribution. In Sec. III D, we discuss the origin of the non-Gaussian behavior.

At a very long time limit, the  $G_s(r, t)$  curves are matched with Gaussian distributions, and relative differences between  $G_s(r, t)$  and  $G_s^{\text{Gauss}}(r, t)$  approach zero.

### C. Non-Gaussian parameter

Deviations from a Gaussian distribution are quantified by a non-Gaussian parameter (NGP). For a 2D system, the NGP is given by [49]

$$\alpha_2(t) = \frac{1}{2} \frac{\langle [\Delta r(t)]^4 \rangle}{\{\langle [\Delta r(t)]^2 \rangle\}^2} - 1, \quad (7)$$

where the moments  $\langle [\Delta r(t)]^n \rangle$  are defined as

$$\langle [\Delta r(t)]^n \rangle = \langle |\mathbf{r}(t) - \mathbf{r}(0)|^n \rangle = \int r^n G_s(\mathbf{r}, t) d\mathbf{r}. \quad (8)$$

Using these two equations, we can see that the NGP is exactly zero for a Gaussian distribution [given by Eq. (2)].

Figures 8(a)–8(c) show the non-Gaussian parameter  $\alpha_2(t)$  for the selected  $\kappa$  and  $\Gamma$  values. The time evolution of the non-Gaussian parameter can be classified into three regimes:

- (i) At short times when dust particles move in the cage created by neighboring dust particles,  $\alpha_2(t)$  is zero.
- (ii) At later times when dust particles escape from the cages and diffuse,  $\alpha_2(t)$  increases with time so that it reaches a peak at intermediate times indicating maximum deviation from the Gaussian. For each  $\kappa$  value, this peak increases with increasing  $\Gamma$  equivalently decreasing  $T$ .
- (iii) At a very long time limit,  $\alpha_2(t)$  decays to zero, as we expected from the Gaussian behavior of  $G_s(r, t)$  at these times.

### D. Self-intermediate scattering function

The quantity of interest in scattering experiments is the spatial Fourier transform of the self-van Hove function, which is called the self-intermediate scattering function (self-ISF) [18],

$$F_s(\mathbf{k}, t) = \int G_s(\mathbf{r}, t) \exp(-i\mathbf{k} \cdot \mathbf{r}) d\mathbf{r}, \quad (9)$$

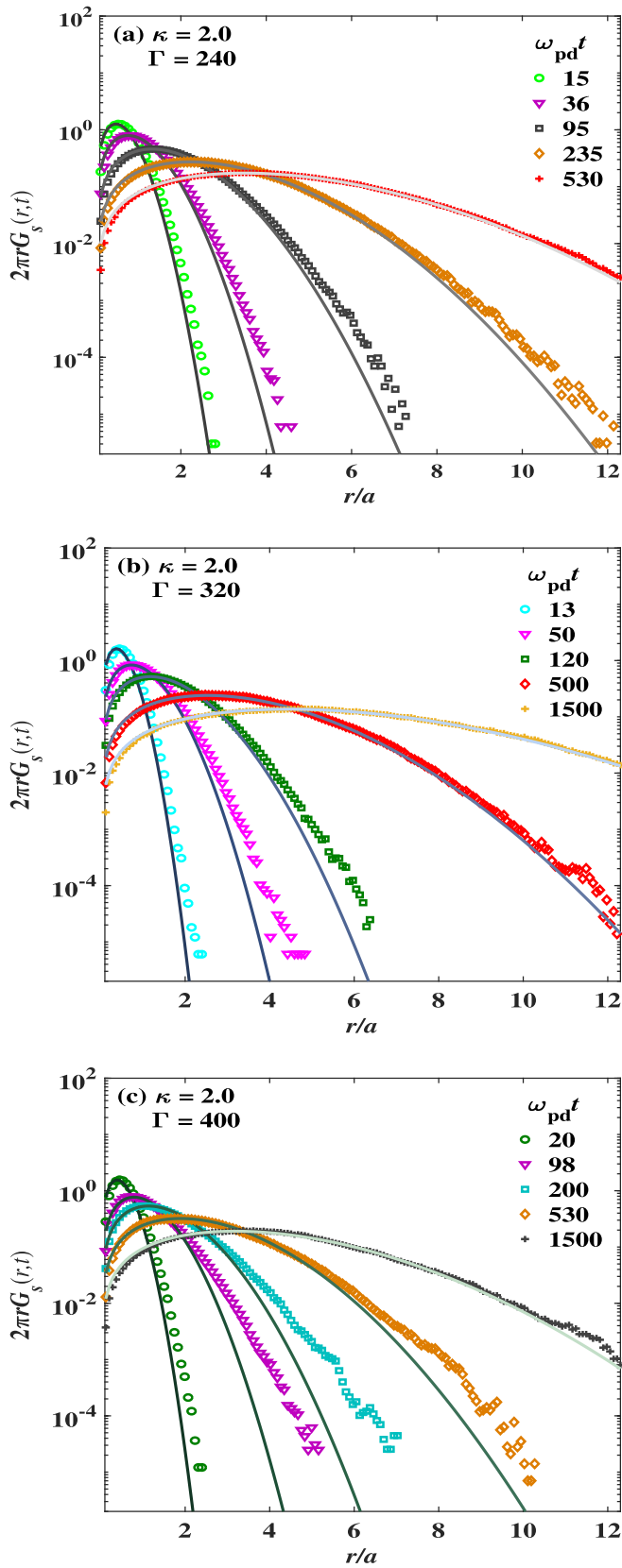


FIG. 2. Time evolution of the self-part of van Hove functions for  $\kappa = 2.0$ . (a)  $\Gamma = 240$ , (b)  $\Gamma = 320$ , and (c)  $\Gamma = 400$ . The symbols are the simulation results, and solid lines are from the Gaussian distribution in Eq. (2) with the MSD obtained from the simulation.

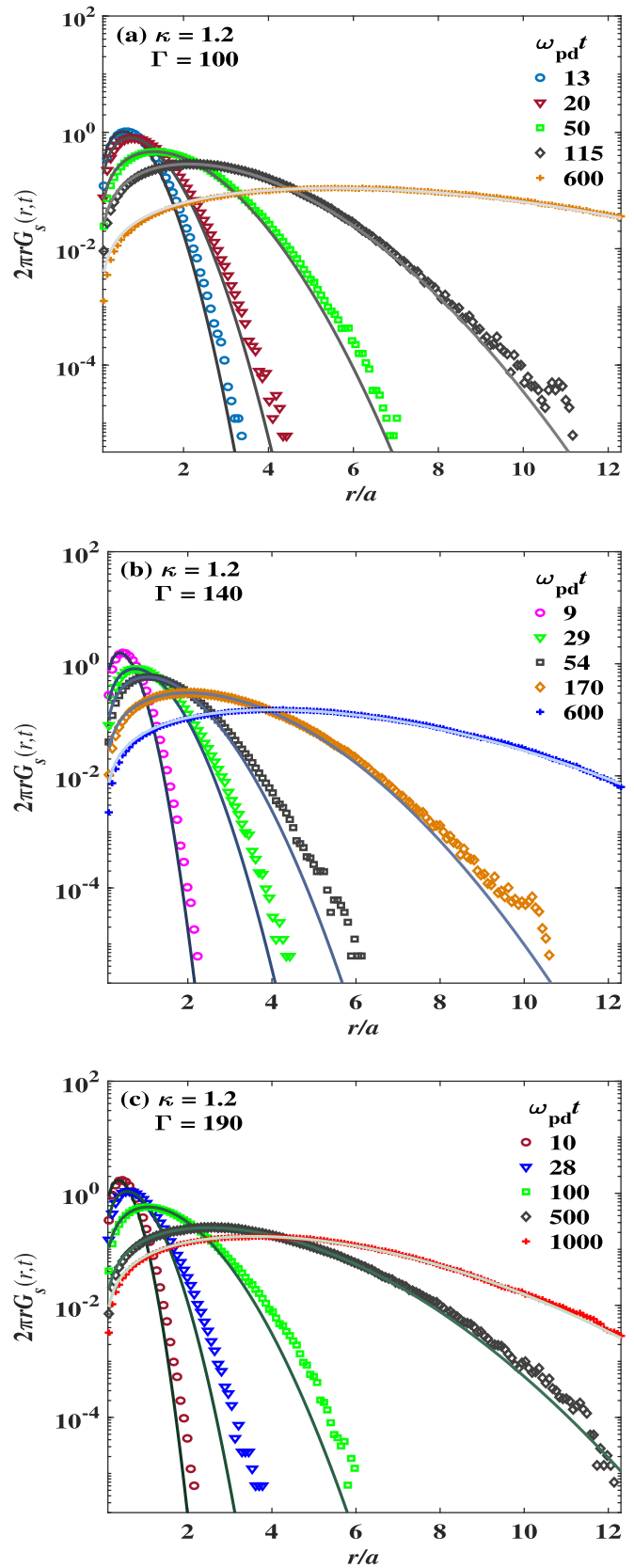


FIG. 3. Time evolution of the self-part of van Hove functions for  $\kappa = 1.2$ . (a)  $\Gamma = 100$ , (b)  $\Gamma = 140$ , and (c)  $\Gamma = 190$ . The symbols are the simulation results, and solid lines are from the Gaussian distribution in Eq. (2) with the MSD obtained from the simulation.

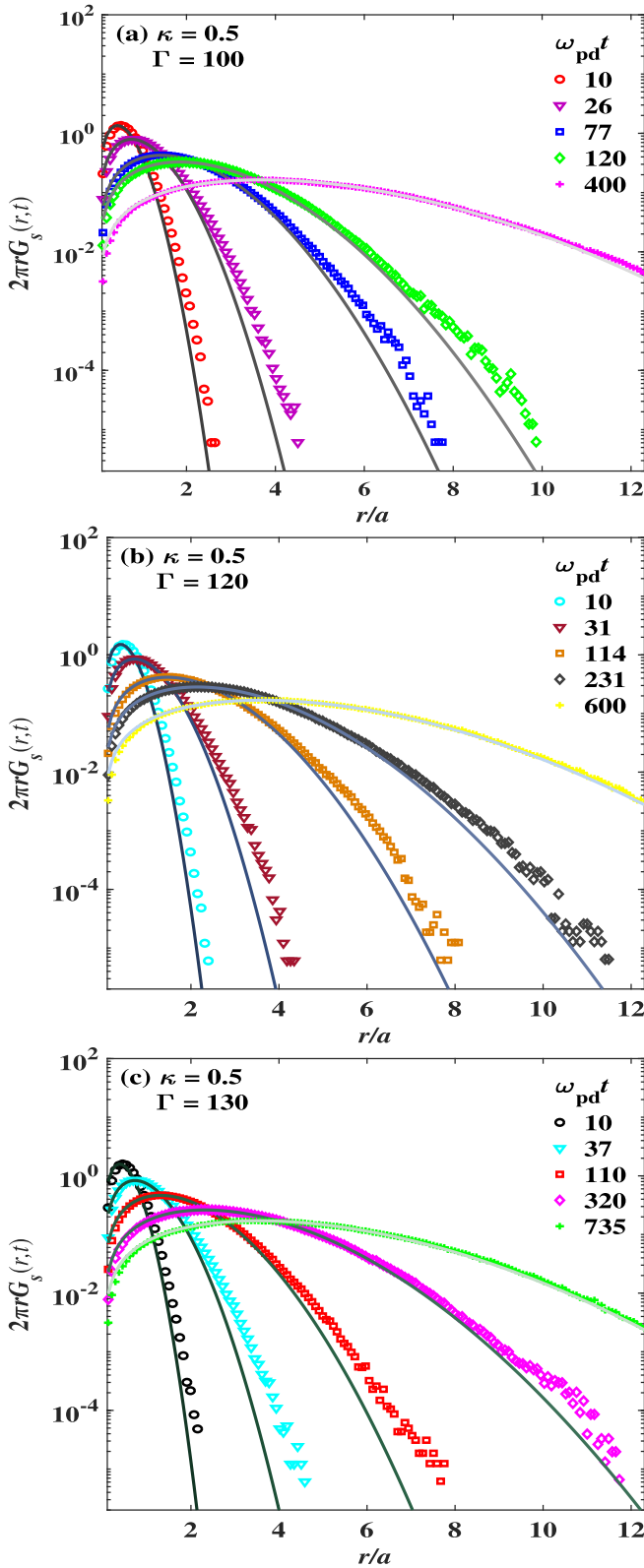


FIG. 4. Time evolution of the self-part of van Hove functions for  $\kappa = 0.5$ . (a)  $\Gamma = 100$ , (b)  $\Gamma = 120$ , and (c)  $\Gamma = 130$ . The symbols are the simulation results, and solid lines are from the Gaussian distribution in Eq. (2) with the MSD obtained from the simulation.

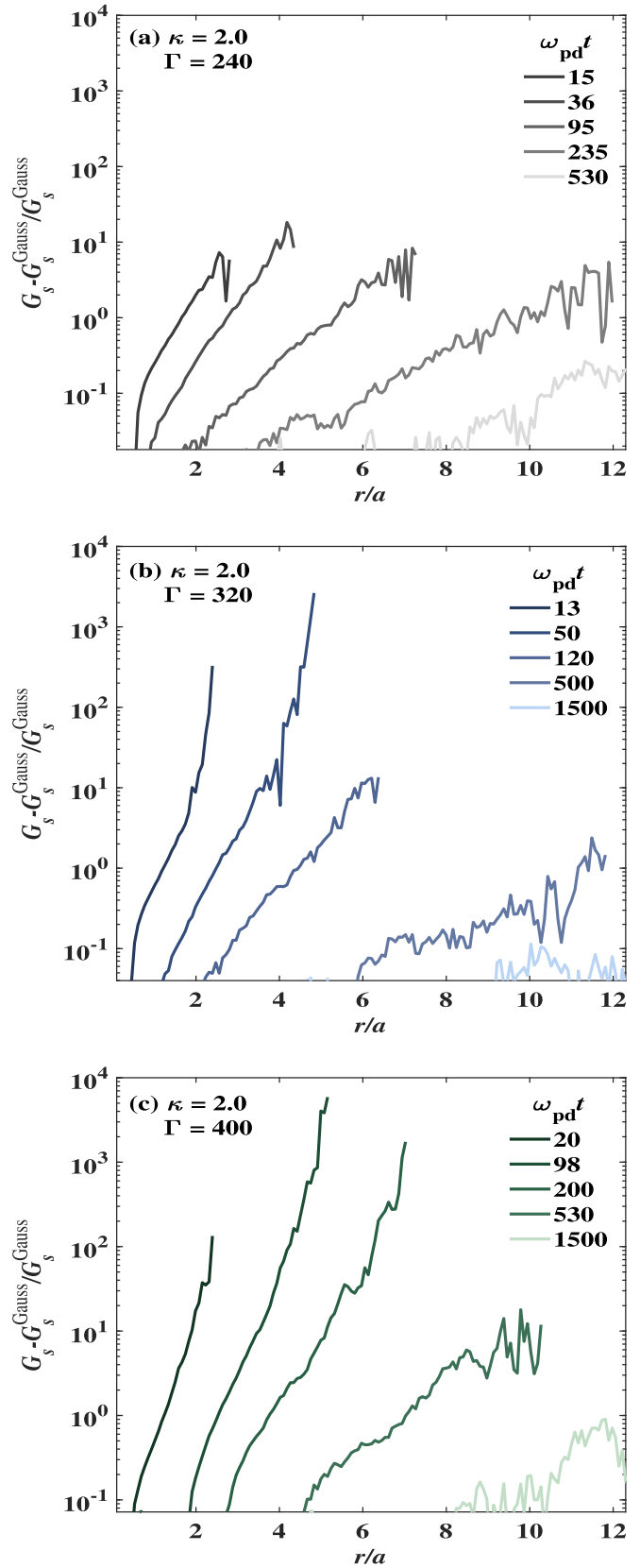


FIG. 5. Relative differences between  $G_s(r,t)$  and Gaussian distribution  $G_s^{\text{Gauss}}(r,t)$  [obtained from Eq. (2)] for (a)  $\Gamma = 240$ , (b)  $\Gamma = 320$ , and (c)  $\Gamma = 400$ .

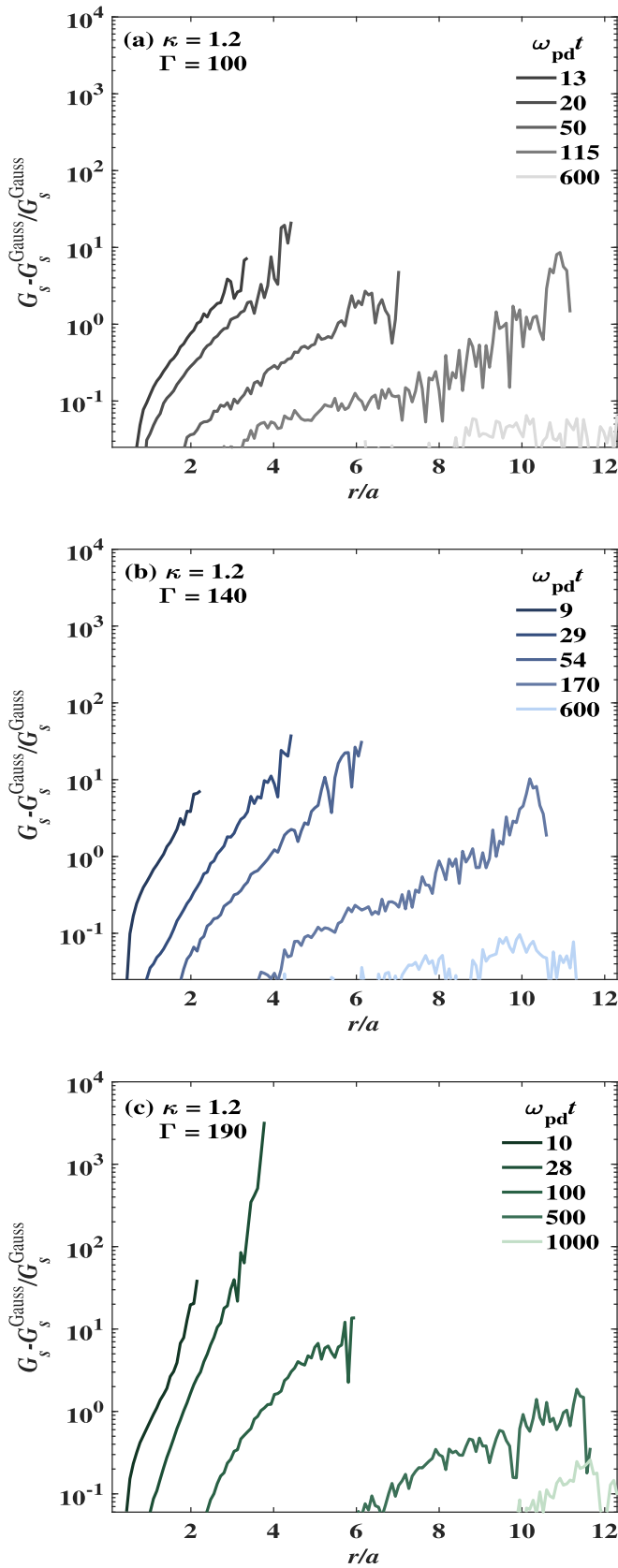


FIG. 6. Relative differences between  $G_s(r, t)$  and Gaussian distribution  $G_s^{\text{Gauss}}(r, t)$  [obtained from Eq. (2)] for (a)  $\Gamma = 100$ , (b)  $\Gamma = 140$ , and (c)  $\Gamma = 190$ .

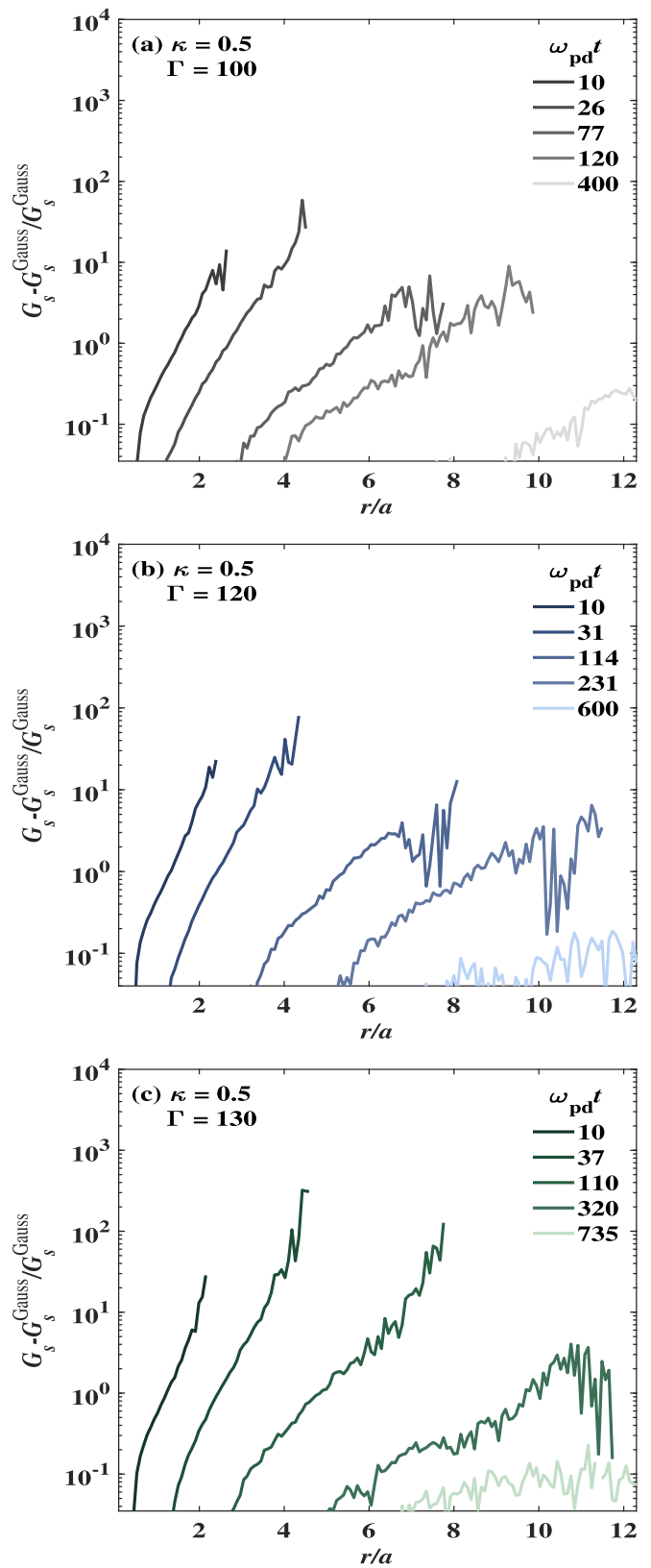


FIG. 7. Relative differences between  $G_s(r, t)$  and Gaussian distribution  $G_s^{\text{Gauss}}(r, t)$  [obtained from Eq. (2)] for (a)  $\Gamma = 100$ , (b)  $\Gamma = 120$ , and (c)  $\Gamma = 130$ .

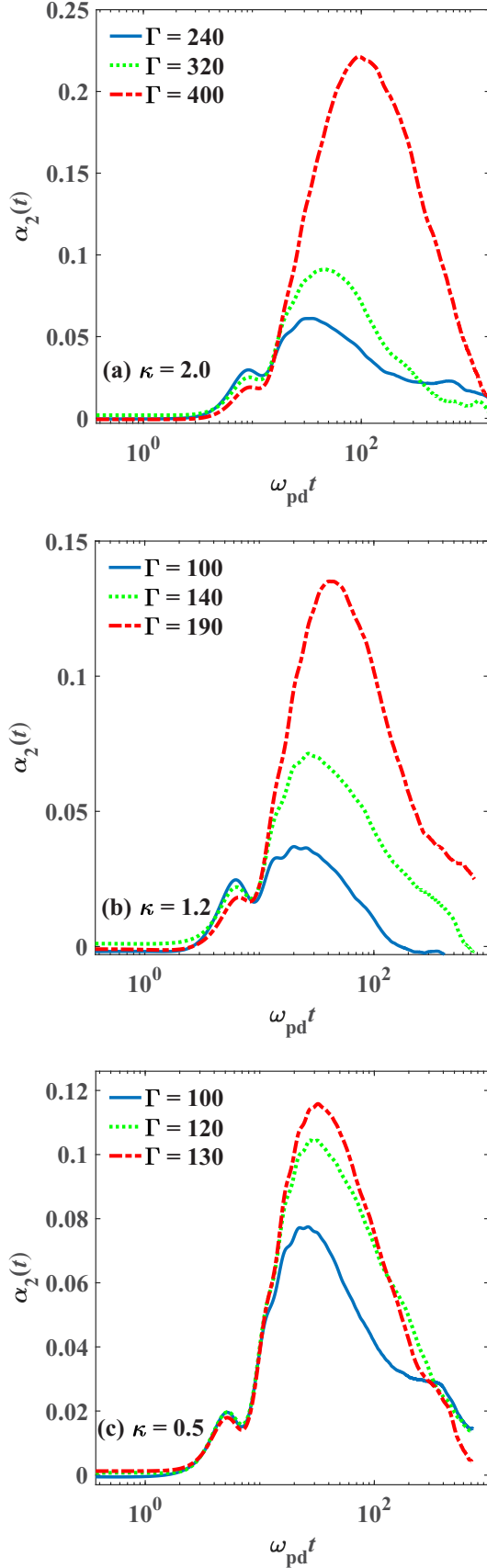


FIG. 8. Non-Gaussian parameter  $\alpha_2(t)$  for different temperatures. (a)  $\kappa = 2.0$ , (b)  $\kappa = 1.2$ , and (c)  $\kappa = 0.5$ . For each  $\kappa$  value, the peak of  $\alpha_2(t)$  increases with increasing  $\Gamma$  or decreasing  $T$ .

where  $\mathbf{k}$  is the 2D wave vector. In the MD simulation with periodic boundaries, the wave vectors are proportional to the periodicity of the system, i.e.,  $\mathbf{k} = (2\pi/L)(k_x, k_y)$ , where  $L$  is the length of the simulation box, and  $k_x, k_y$  are integers [50]. The function  $F_s(\mathbf{k}, t)$  is interpreted as the characteristic function of  $G_s(\mathbf{r}, t)$  because according to the probability theory, the Fourier transform of a probability distribution function is called the characteristic function of the distribution [51]. Using the definition of the self-van Hove function from Eq. (4) and applying the property of the  $\delta$  function gives

$$F_s(\mathbf{k}, t) = \frac{1}{N} \left\langle \sum_{i=1}^N \exp\{-i\mathbf{k} \cdot [\mathbf{r}_i(t) - \mathbf{r}_i(0)]\} \right\rangle. \quad (10)$$

For an isotropic system,  $F_s(\mathbf{k}, t)$  depends only on the magnitude  $k = |\mathbf{k}|$ , therefore averaging over all directions yields

$$\langle \exp(-i\mathbf{k} \cdot \mathbf{r}) \rangle_\phi = \frac{1}{2\pi} \int_0^{2\pi} \exp(-ikr \cos \phi) d\phi = J_0(kr), \quad (11)$$

where  $\phi$  is the angle between the vectors  $\mathbf{k}$  and  $\mathbf{r}$ , and  $J_0(kr) = \sin(kr)/(kr)$  is the ordinary Bessel function of order zero. Therefore, for an isotropic system,  $F_s(k, t)$  reduces to

$$F_s(k, t) = \frac{1}{N} \left\langle \sum_{i=1}^N \frac{\sin(k|\mathbf{r}_i(t) - \mathbf{r}_i(0)|)}{k|\mathbf{r}_i(t) - \mathbf{r}_i(0)|} \right\rangle. \quad (12)$$

We computed  $F_s(k, t)$  from Eq. (12) for various wave numbers  $k$  and the selected  $\kappa$  and  $\Gamma$  values. The results are shown in Figs. 9(a)–9(i). If the system exhibits Fickian diffusion, the self-van Hove function is Gaussian at all times and its Fourier transform is obtained by substituting Eq. (2) in Eq. (9) as follows:

$$F_s(k, t) = \exp\left(-\frac{k^2 \langle [\Delta r(t)]^2 \rangle}{4}\right), \quad (13)$$

which is known as the Gaussian approximation [18]. As shown in Figs. 9(a)–9(i), by comparing the self-ISF obtained by simulations and the corresponding Gaussian approximation, i.e., Eq. (13), in which  $\langle [\Delta r(t)]^2 \rangle$  is determined from the simulation data, we find that at intermediate times, the Gaussian approximation fails to describe the diffusion of dust particles, indicating the non-Gaussian dynamics in 2D Yukawa liquids. At short and very long times, as we expected, the Gaussian approximation is a good description for the self-intermediate scattering function.

The origin of this non-Gaussian behavior may be heterogeneous dynamics, which has been observed in liquids [52,53]. Dynamical heterogeneity reflects the existence of regions in which dust particles are more mobile than expected from a Gaussian approximation, that is, dust particles that move faster than the rest. These dust particles form clusters, i.e., groups of the particles, and they move along stringlike (one-dimensional) paths. Therefore, strings of mobile dust particles flow among regions including less mobile dust particles [13]. As a result, the displacement deviations appear over time and the distribution function of the particle displacement, i.e.,  $G_s$ , departs from a Gaussian shape. Consequently,  $\alpha_2(t)$  is not zero.

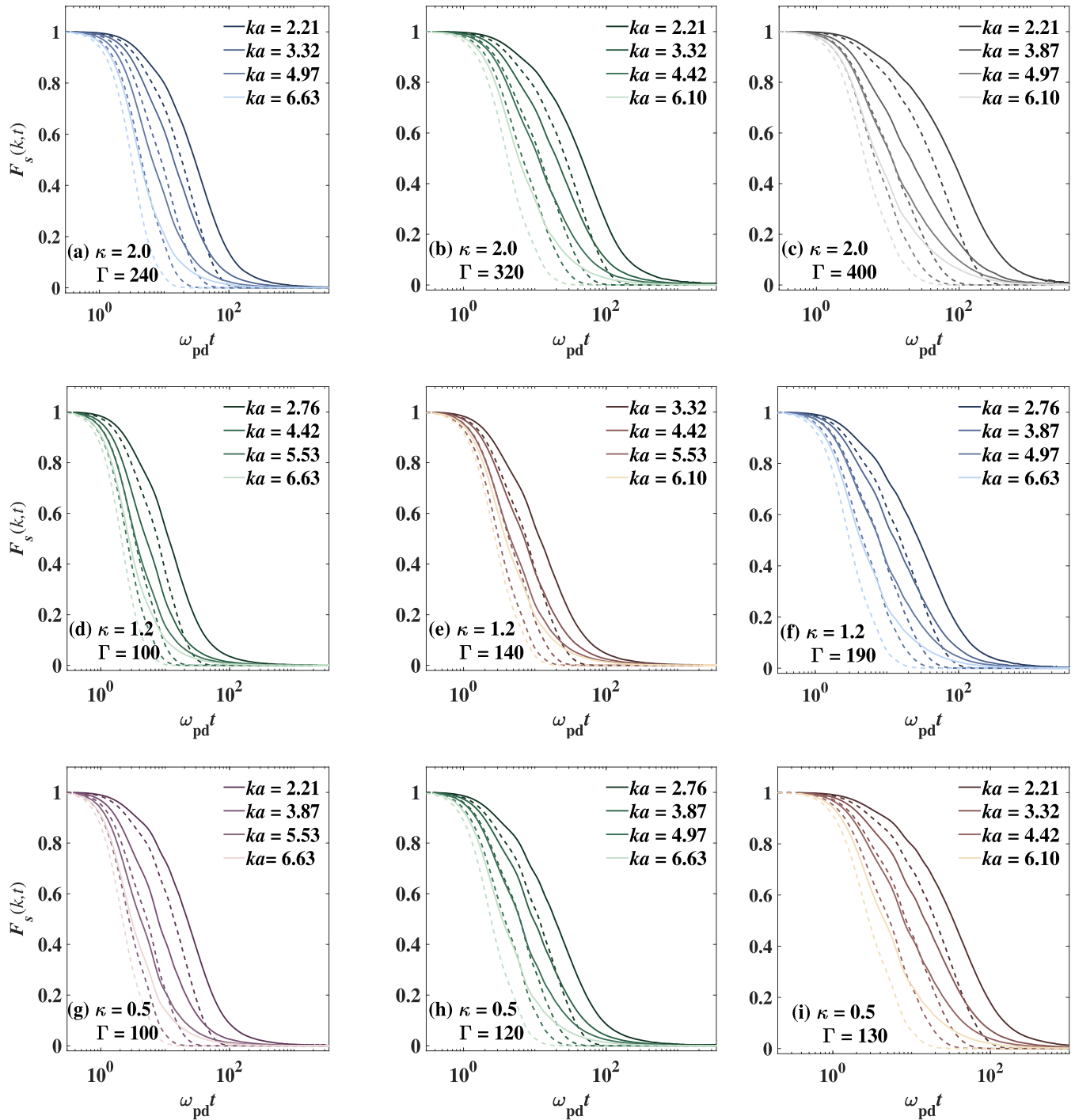


FIG. 9. Self-part of the intermediate scattering functions  $F_s(k, t)$  for various dimensionless wave numbers  $ka$  and the selected  $\Gamma$  and  $\kappa$  values: [(a)–(c)]  $\kappa = 2.0$ , [(d)–(f)]  $\kappa = 1.2$ , and [(g)–(i)]  $\kappa = 0.5$ . Solid lines are from the simulation, and dashed lines are from the Gaussian approximation obtained from Eq. (13) with the MSD obtained from the simulation.

**IV. SUMMARY AND CONCLUSIONS**

We have investigated the dynamics of dust particles in two-dimensional Yukawa liquids using molecular dynamics simulation. First, we have computed the mean-squared displacement on the allowed ranges of experimental parameters, and we have shown that it is linear with time (Fickian diffusion) in very low temperatures, on the timescales at which dust particles diffuse. Then, we have computed the distribution of

the particle displacements  $G_s(r, t)$ , and we have compared it with  $G_s(r, t)$  obtained from the Gaussian approximation. Significantly, we found that at intermediate times, the distribution of the particle displacement deviates from the Gaussian, i.e., the failure of the Gaussian approximation, which states that when diffusion is Fickian, the distribution of particle displacement is Gaussian. This result may be attributed to the heterogeneous dynamics of dust particles in Yukawa liquids. The non-Gaussian parameter and the self-intermediate

scattering function have also been computed, and their results have confirmed these deviations. Furthermore, we found that the deviations increase as the temperature of the liquid decreases. Here, we have decreased the temperature to near the melting point  $T_m$ , where the liquid phase is maintained.

A further decrease in temperature results in a phase change of the system from liquid to solid. Investigating the non-Gaussian behavior and the degree of deviation from Gaussian in Yukawa solids can be an interesting research topic. Our future work will include this research.

- [1] M. Bonitz, N. Horing, and P. Ludwig, *Introduction to Complex Plasmas* (Springer, Berlin, 2010).
- [2] V. E. Fortov, A. V. Ivlev, S. A. Khrapak, A. G. Khrapak, and G. E. Morfill, *Phys. Rep.* **421**, 1 (2005).
- [3] G. E. Morfill and A. V. Ivlev, *Rev. Mod. Phys.* **81**, 1353 (2009).
- [4] A. G. Khrapak and S. A. Khrapak, *Phys. Plasmas* **25**, 034502 (2018).
- [5] Y. Feng, J. Goree, and B. Liu, *Phys. Rev. E* **87**, 013106 (2013).
- [6] Y. Feng, J. Goree, B. Liu, L. Wang, and W. Tian, *J. Phys. D* **49**, 235203 (2016).
- [7] K. Wang, D. Huang, and Y. Feng, *J. Phys. D* **51**, 245201 (2018).
- [8] Y. Feng, W. Lin, and M. S. Murillo, *Phys. Rev. E* **96**, 053208 (2017).
- [9] H. Yukawa, *Proc. Phys.-Math. Soc. Jpn.* **17**, 48 (1935).
- [10] U. Konopka, G. E. Morfill, and L. Ratke, *Phys. Rev. Lett.* **84**, 891 (2000).
- [11] Y. Feng, J. Goree, and B. Liu, *Phys. Rev. Lett.* **100**, 205007 (2008).
- [12] P. Hartmann, A. Z. Kovács, A. M. Douglass, J. C. Reyes, L. S. Matthews, and T. W. Hyde, *Phys. Rev. Lett.* **113**, 025002 (2014).
- [13] B. Liu, J. Goree, and O. S. Vaulina, *Phys. Rev. Lett.* **96**, 015005 (2006).
- [14] R. Brown, *Philos. Mag.* **4**, 161 (1828).
- [15] A. Einstein, *Ann. Phys. (Leipzig)* **322**, 549 (1905).
- [16] A. V. Chechkin, F. Seno, R. Metzler, and I. M. Sokolov, *Phys. Rev. X* **7**, 021002 (2017).
- [17] L. van Hove, *Phys. Rev.* **95**, 249 (1954).
- [18] J. Hansen and I. R. McDonald, *Theory of Simple Liquids* (Academic Press, London, 2006).
- [19] J. M. Haile, *Molecular Dynamics Simulation: Elementary Methods* (Wiley, New York, 1992).
- [20] B. Liu and J. Goree, *Phys. Rev. E* **75**, 016405 (2007).
- [21] T. Ott, M. Bonitz, Z. Donkó, and P. Hartmann, *Phys. Rev. E* **78**, 026409 (2008).
- [22] P. Hartmann, J. C. Reyes, E. G. Kostadinova, L. S. Matthews, T. W. Hyde, R. U. Masheeva, K. N. Dzhumagulova, T. S. Ramazanov, T. Ott, H. Kählert, M. Bonitz, I. Korolov, and Z. Donkó, *Phys. Rev. E* **99**, 013203 (2019).
- [23] Y. Feng, J. Goree, and B. Liu, *Phys. Rev. E* **82**, 036403 (2010).
- [24] W.-T. Juan and Lin I, *Phys. Rev. Lett.* **80**, 3073 (1998).
- [25] O. S. Vaulina and I. E. Dranzhevski, *Phys. Scr.* **73**, 577 (2006).
- [26] Z. Donkó, J. Goree, P. Hartmann, and B. Liu, *Phys. Rev. E* **79**, 026401 (2009).
- [27] S. Nunomura, D. Samsonov, S. Zhdanov, and G. Morfill, *Phys. Rev. Lett.* **96**, 015003 (2006).
- [28] L.-J. Hou, A. Piel, and P. K. Shukla, *Phys. Rev. Lett.* **102**, 085002 (2009).
- [29] Y. Feng, J. Goree, B. Liu, T. P. Intrator, and M. S. Murillo, *Phys. Rev. E* **90**, 013105 (2014).
- [30] W.-T. Juan, M.-H. Chen, and Lin I, *Phys. Rev. E* **64**, 016402 (2001).
- [31] K. N. Dzhumagulova, R. U. Masheeva, T. S. Ramazanov, and Z. Donkó, *Phys. Rev. E* **89**, 033104 (2014).
- [32] G. Kwon, B. J. Sung, and A. Yethiraj, *J. Phys. Chem. B* **118**, 8128 (2014).
- [33] S. K. Schnyder, T. O. E. Skinner, A. L. Thorneywork, D. G. A. L. Aarts, J. Horbach, and R. P. A. Dullens, *Phys. Rev. E* **95**, 032602 (2017).
- [34] J. Kim, C. Kim, and B. J. Sung, *Phys. Rev. Lett.* **110**, 047801 (2013).
- [35] J. Guan, B. Wang, and S. Granick, *ACS Nano* **8**, 3331 (2014).
- [36] K. He, F. B. Khorasani, S. T. Retterer, D. K. Thomas, J. C. Conrad, and R. Krishnamoorti, *ACS Nano* **7**, 5122 (2013).
- [37] K. He, S. T. Retterer, B. R. Srijanto, J. C. Conrad, and R. Krishnamoorti, *ACS Nano* **8**, 4221 (2014).
- [38] D. Frenkel and B. Smit, *Understanding Molecular Dynamics Simulation* (Academic Press, San Diego, 2002).
- [39] H. Ohta and S. Hamaguchi, *Phys. Plasmas* **7**, 4506 (2000).
- [40] G. J. Kalman, P. Hartmann, Z. Donkó, and M. Rosenberg, *Phys. Rev. Lett.* **92**, 065001 (2004).
- [41] Z. Donkó, J. Goree, P. Hartmann, and K. Kutasi, *Phys. Rev. Lett.* **96**, 145003 (2006).
- [42] P. Hartmann, G. J. Kalman, Z. Donkó, and K. Kutasi, *Phys. Rev. E* **72**, 026409 (2005).
- [43] Y. Feng, W. Li, Q. Wang, and W. Lin, *Phys. Plasmas* **23**, 113705 (2016).
- [44] S. Nosé, *J. Chem. Phys.* **81**, 511 (1984).
- [45] W. G. Hoover, *Phys. Rev. A* **31**, 1695 (1985).
- [46] W. C. Swope, H. C. Andersen, P. H. Berens, and K. R. Wilson, *J. Chem. Phys.* **76**, 637 (1982).
- [47] B. L. Holian, A. F. Voter, and R. Ravelo, *Phys. Rev. E* **52**, 2338 (1995).
- [48] T. J. Feder, I. Brust-Mascher, J. P. Slattery, B. Baird, and W. W. Webb, *Biophys. J.* **70**, 2767 (1996).
- [49] A. Rahman, *Phys. Rev.* **136**, A405 (1964).
- [50] M. P. Allen and D. J. Tildesley, *Computer Simulation of Liquids* (Oxford University Press, Oxford, 2017).
- [51] B. J. Berne and R. Pecora, *Dynamic Light Scattering: With Applications to Chemistry, Biology and Physics* (Wiley, New York, 1976).
- [52] C. Reichhardt and C. J. Olson Reichhardt, *Phys. Rev. Lett.* **90**, 095504 (2003).
- [53] W. Kob, C. Donati, S. J. Plimpton, P. H. Poole, and S. C. Glotzer, *Phys. Rev. Lett.* **79**, 2827 (1997).